RSC Advances

PAPER

View Article Online
View Journal | View Issue

Cite this: *RSC Adv.*, 2021, **11**, 12710

The improvement in hole-transporting and electroluminescent properties of diketopyrrolopyrrole pigment by grafting with carbazole dendrons†

Wipaporn Kitisriworaphan,[a] Thanyarat Chawanpunyawat,[b] Thanaporn Manyum,[a] Pongsakorn Chasing,[b] Supawadee Namuangruk,[c] Taweesak Sudyoadsuk[b] and Vinich Promarak *[bd]

Diketopyrrolopyrrole (DPP) pigments are essential and have been intensively exploited as building-blocks for the synthesis of organic semiconducting polymers and small molecules; however, DPP derivatives as emissive materials for electroluminescent (EL) devices have rarely been explored. In this work, a series of new DPP derivatives grafted with carbazole dendrons in a non-conjugated fashion using an amide linkage was designed to improve the performance of DPP in EL devices. Three DPP derivatives (**G0DPP**, **G1DPP** and **G2DPP**) bearing di(*p*-chlorophenyl)-DPP (Pigment Red 254) as the core substituted with a hexyl chain, *N*-hexyl carbazole and *N*-hexyl-*N*′-9,3′:6′,*N*″-tercarbazole, respectively, were synthesized to afford improved hole-transporting properties without affecting the photophysical and electronic properties of the DPP core. The synthesized DPP derivatives displayed an intense yellow fluorescence emission peaked at 536 nm with an absolute photoluminescence quantum yield close to unity in solution. The hole-transporting capability of molecules was improved when carbazole dendrons were incorporated, which increased with an increase in the generation of substituent carbazole dendrons in the order of **G0DPP** < **G1DPP** < **G2DPP**. Significantly, the use of **G2DPP**, showing the highest hole mobility, in an EL device yielded a strong and stable yellow emission peaked at 556 nm (CIE *x*, *y* color coordinates of (0.45, 0.53)) with a brightness of 3060 cd m^{-2}, maximum luminous efficiency of 9.24 cd A^{-1} and a maximum EQE of 3.11%.

Received 30th January 2021
Accepted 15th March 2021

DOI: 10.1039/d1ra00805f

rsc.li/rsc-advances

Introduction

The application of organic materials in organic light-emitting diodes (OLEDs) received significant interest due to their successful application in full-color displays (mobile phones, digital cameras, and televisions) and potential use as solid-state lighting sources after it was first reported by Tang and Vanslyke in 1987.[1–5] To realize highly efficient electroluminescent (EL) performances in OLED devices, thermally evaporated multilayer devices integrated with efficient charge injection and charge transporting layers are fabricated.[6–8] Conversely, solution processing can offer simpler and more cost-effective processing and is suitable for large-area roll-to-roll production.[9] Nonetheless, the further advancement of solution-processed OLED performances is still very challenging for competitive lighting devices. One key aspect for achieving high-performance OLEDs is the design and synthesis of advanced light-emitting materials with suitable electrical and optical properties to fully use excitons for efficient energy conversion, which is still a challenge.[10–12]

Diketopyrrolopyrroles (DPPs) are a family of high-performance industrial pigments with remarkable thermal stability and excellent photostability.[13] They have been widely used as high-performance pigments such as inks, paints, and plastics.[13] Furthermore, these characteristics are also desirable for active materials in mass-producible low-cost organic electronics.[14] DPPs have several advantages, for example, they are strong acceptors that exhibit a high molar absorption coefficient and high fluorescence quantum yield (Φ_{PL}) and can undergo several synthetic modifications.[15] Thus, based on these features, in recent years DPPs have emerged as one of the most

[a]*School of Chemistry, Institute of Science, Suranaree University of Technology, Muang District, Nakhon Ratchasima 30000, Thailand*

[b]*Department of Materials Science and Engineering, School of Molecular Science and Engineering, Vidyasirimedhi Institute of Science and Technology, Wangchan, Rayong 21210, Thailand. E-mail: vinich.p@vistec.ac.th*

[c]*National Nanotechnology Center (NANOTEC), National Science and Technology Development Agency, Pathum Thani 12120, Thailand*

[d]*Research Network of NANOTEC-VISTEC on Nanotechnology for Energy, Vidyasirimedhi Institute of Science and Technology, Wangchan, Rayong 21210, Thailand*

† Electronic supplementary information (ESI) available. See DOI: 10.1039/d1ra00805f

successful building blocks in polymers, oligomers, and small molecules for the synthesis of high-mobility transistor materials,[16–20] sensing materials,[21–24] bioimaging fluorescent probes,[25,26] two-photon absorption materials[27,28] and materials for the fabrication of photovoltaic devices.[29–32] Many efficient donor and acceptor materials used in high-performance organic photovoltaics (OPV) are derivatives of DPP.[33–36] However, despite their intense emission in solution, DPP derivatives as emissive materials in OLEDs are found to be rare.[37–41] Most of them are DPP-containing polymers, but the small DPP molecule has not been investigated to date. This is because the planar structure of DPP induces strong intermolecular π–π stacking, leading to dissipative intermolecular charge transfer, aggravated charge recombination, and low fluorescence emission in the solid state.

Hence, in this work, we report our attempt to design efficient emissive materials based on DPP for application in solution-processed OLEDs. As depicted in Scheme 1, di(*p*-chlorophenyl)-DPP (Pigment Red 254) was utilized as the DPP emissive core owing to its strong fluorescence emission and inexpensive commercial availability.[42] The carbazole dendron was chosen as the grafting moiety given that the carbazole unit has a high triplet energy (3.0 eV)[43] and excellent hole-transporting ability. Carbazole has also been extensively exploited as a building block for the design of wide-band-gap host materials[44,45] and multifunctional phosphors.[46–48] Additionally, the carbazole dendron was varied to tune the properties of the molecule. Besides, carbazole dendrons have been effectively used to construct many highly efficient hole-transporting materials[49–51] and hole-transporting light-emitting materials[52–54] for OLEDs. Meanwhile, an alkyl linkage was selected to connect the nitrogen atoms in the DPP unit and dendron, aiming to retain the optical and electronic properties of DPP and achieve convenient synthesis. The hexyl chain was favourably used because longer chains may separate the dendron and core too far from each other, resulting in reduced effects (energy transfer or electron transfer) between the two moieties, while shorter chains may cause some difficulties in the synthesis. It has been reported that carbazole-containing alkyl bromide is unstable, and thus undergoes elimination reactions to form inactive olefins.[55] The hexyl linkage would also give decent solubility to the dendrimers in common organic solvents, allowing the materials to be fabricated *via* solution-based processes. Thus, employing this design strategy, we achieved the synthesis of efficient green phosphorescent iridium dendrimers, where the affixing carbazole dendrons were anticipated to improve the hole-transporting capability and function as a host for the iridium emissive core. Accordingly, furnishing high and balanced charge carrier ability to the materials should pave the way to improve the EL performance of

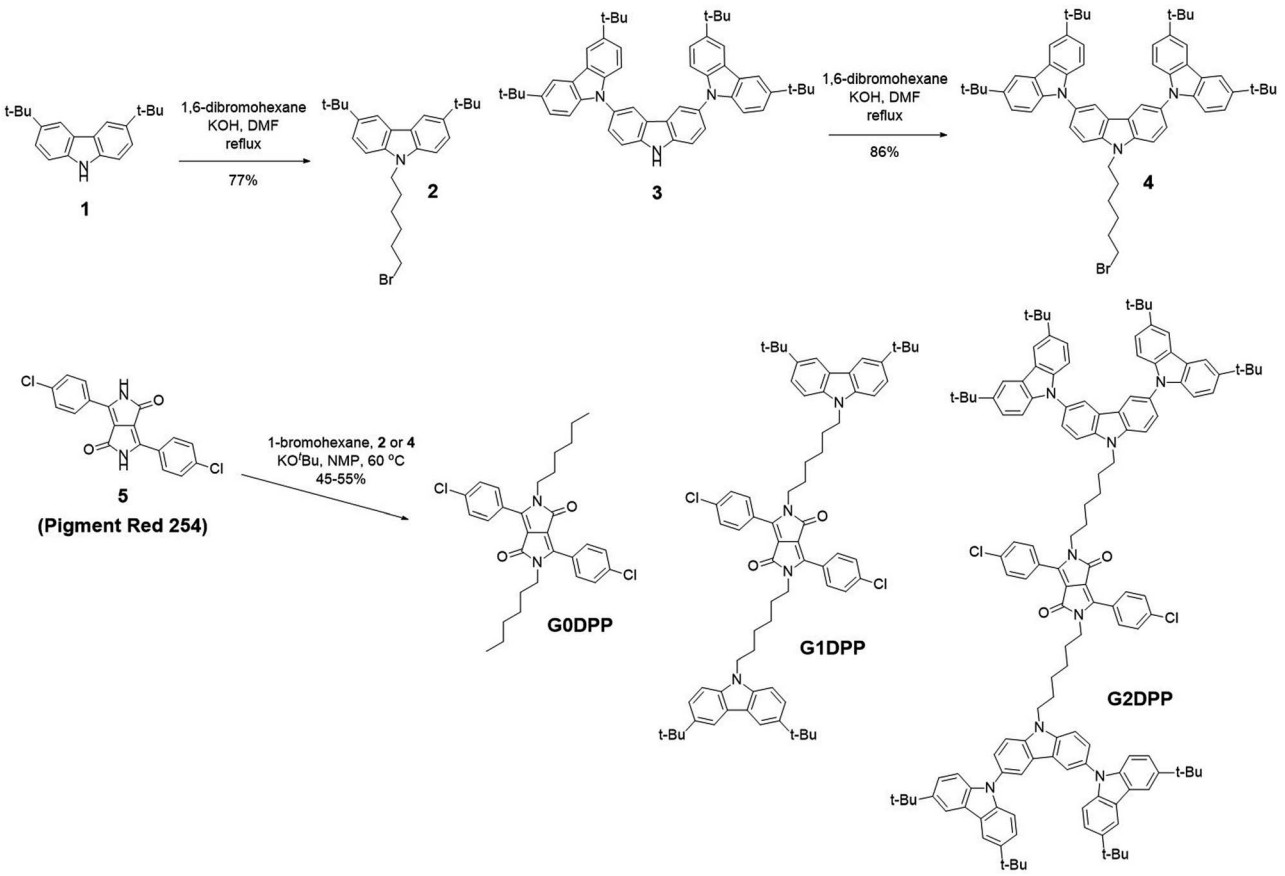

Scheme 1 . Synthesis of diketopyrrolopyrrole derivatives (G0DPP–G2DPP).

DPP-based OLEDs. Indeed, the **G2DPP**-based device achieved the best EL performance with a strong and stable yellow emission with CIE x, y color coordinates of (0.45, 0.53) and EQE as high as 3.11% (9.24 cd A^{-1}).

Experimental

Materials and methods

All chemicals were supplied and used as received without further purification. Pigment Red 254 was obtained from Tokyo Chemical Industry (TCI) Chemicals. 3,6-Di-*tert*-butylcarbazole (**1**) and 3,3″,6,6″-tetra-*tert*-butyl-*N*′,3′:6′,*N*″-tercarbazole (**3**) were synthesized following the literature methods.[50,52]

^{1}H and ^{13}C NMR spectra were acquired on a Bruker Ascend III (600 MHz) spectrometer in $CDCl_3$ solvent. High-resolution mass spectra were analyzed using a Bruker Autoflex Speed mass spectrometer. Infrared spectra were recorded on a Perkin Elmer FTIR spectrophotometer. UV-Vis absorption spectra were measured using a Perkin Elmer Lambda 1050 UV/Vis/NIR spectrometer. AFM images were taken using a Park System model NX-10 instrument operated in the tapping mode under ambient conditions. TGA analyses were performed using a Perkin-Elmer TGA Pyris 1 instrument at a heating rate of 10 °C min^{-1} under an N_2 flow. PL spectra and decay profiles were obtained using an Edinburgh Instruments FLS980 spectrometer. Absolute photoluminescence quantum yields (Φ_{PL}) were measured on an Edinburgh Instruments FLS980 spectrometer integrated with a calibrated integrating sphere. Electrochemical analyses were done on an Autolab PGSTA101 with a three-electrode setup (Pt, glassy carbon, and Ag/AgCl) in CH_2Cl_2 and *n*-Bu_4NPF_6 (0.1 M) as the supporting electrolyte. Melting points were measured using a Krüss KSP1N melting point meter and are uncorrected.

Quantum chemical calculations were performed using the Gaussian 09 software.[56] The ground-state geometries, HOMO and LUMO distributions, and HOMO, LUMO energy levels were calculated using the B3LYP/6-31G (d,p) basis set in CH_2Cl_2 solvent.

OLED devices (ITO/PEDOT:PSS (35 nm)/EML (35 nm)/TAZ (40 nm)/LiF (0.5 nm) : Al (150 nm)) were fabricated on patterned ITO glass substrates (12 Ω sq^{-1}). The substrates were pre-cleaned carefully and cured with UV/O_3 for 2 min. As the hole injection layer, a 40 nm-think PEDOT:PSS thin film was spin-coated on top from a 1.2 wt% aqueous dispersion of PEDOT:PSS (CLEVIOSTM P VP Al 4083) at a spinning speed of 5000 rpm for 30 s followed by drying at 120 °C for 15 min. Subsequently, thin films with a thickness of 35 nm of **G0DPP–G2DPP** 3 wt% in mCP host as the EML were spin-coated on top from toluene solution of EML (2% w/v) at a spin speed of 2500 rpm for 30 s. The thickness of all the spin-coated films was assessed using a Dektak XTL stylus profiler. Then TAZ as an electron transporting layer of 40 nm, LiF of 0.5 nm, and aluminum of 150 nm were thermally evaporated using a Kurt J. Lasker Mini SPECTROS 100 thin film deposition system. The thin film thicknesses were monitored and controlled using a quartz crystal. All devices were unencapsulated and measured under ambient conditions in the dark. They were analyzed using a Keithley 2400 source meter, a Hamamatsu Photonics PMA-12 multi-channel analyzer, and an integrating sphere equipped with a Hamamatsu Photonics C9920-12 EQE Measurement System.

Synthesis and characterization

***N*-(6-Bromohexyl)-3,6-di-*tert*-butyl-carbazole (2).** 1,6-Dibromohexane (2.8 mL, 18.0 mmol) was added to a solution of compound **1** (1.0 g, 3.6 mmol) and KOH (0.81 g, 14.4 mmol) in DMF (50 mL) at 0 °C. The mixture was stirred at room temperature for 24 h and then diluted with water (100 mL) and extracted with CH_2Cl_2 (3 × 50 mL). The combined organic layer was washed with water (50 mL), brine solution (50 mL), dried over anhydrous Na_2SO_4, filtered and concentrated under reduced pressure. The crude product was purified by column chromatography (CH_2Cl_2/hexane) to afford a white solid (1.22 g, 77%). Mp 120–122 °C; FTIR (ATR, cm^{-1}) ν 2937, 2842, 1482, 1376, 1074, 831, 694. ^{1}H-NMR (600 MHz, $CDCl_3$, ppm) δ 8.10 (s, 2H), 7.50 (d, J = 8.4 Hz, 2H), 7.30 (d, J = 8.4 Hz, 2H), 4.25 (t, J = 7.2 Hz, 2H), 3.36 (t, J = 6.6 Hz, 2H), 1.81–1.90 (m, 4H), 1.44 (s, 18H), 1.41–1.39 (m, 4H); ^{13}C-NMR (150 MHz, $CDCl_3$, ppm) δ 141.5, 139.0, 123.3, 122.7, 116.3, 108.0, 43.0, 34.7, 33.7, 32.6, 32.4, 32.1, 29.0, 28.0, 26.5; *m*/*z* (HRMS MALDI-TOF) $C_{26}H_{36}BrN$ calcd 441.2031; found 441.3331 (M+).

***N*-(6-Bromohexyl)-3,3″,6,6″-tetra-*tert*-butyl-N′,3′:6′,N″-tercarbazole (4).** It was synthesized from compound **3** using the same conditions as that for **2** and obtained as a white solid (1.06 g, 86%). Mp 293–295 °C; FTIR (ATR, cm^{-1}) ν 2935, 2847, 1485, 1375, 1074, 831, 694. ^{1}H-NMR (600 MHz, $CDCl_3$, ppm) δ 8.18 (s, 2H), 8.15 (s, 4H), 7.64 (m, 4H), 7.44 (m, 4H), 7.31 (m, 4H), 4.49 (t, J = 7.2 Hz, 2H), 3.43 (m, 2H), 2.09–1.91 (m, 4H), 1.46 (s, 36H), 1.44 (m, 4H) ppm; ^{13}C-NMR (150 MHz, $CDCl_3$, ppm) δ 142.5, 140.3, 139.9, 129.9, 125.7, 123.5, 123.4, 123.0, 119.5, 116.2, 109.9, 109.1, 43.5, 34.7, 33.7, 32.6, 31.9, 29.1, 28.0, 27.3, 26.6 ppm; *m*/*z* (HRMS MALDI-TOF) $C_{58}H_{66}BrN_3$ calcd 883.4440; found 883.605 (M+).

3,6-Bis(4-chlorophenyl)-2,5-dihexyl-2,5-dihydropyrrolo[3,4-*c*]pyrrole-1,4-dione (G0DPP). Pigment Red 254 (**5**) (0.10 g, 0.28 mmol), KO^{t}Bu (0.0691 g, 0.62 mmol) and NMP (15 mL) were heated to 60 °C. 1-Bromohexane (0.12 mL, 0.84 mmol) was then added, and the mixture was stirred at 60 °C for 18 h. After cooling to room temperature, it was diluted with water (50 mL) and extracted with CH_2Cl_2 (3 × 50 mL). The combined organic layer was washed with water (50 mL), brine solution (50 mL), dried over anhydrous Na_2SO_4, filtered and concentrated under reduced pressure. The crude product was purified by column chromatography (CH_2Cl_2/hexane) to afford an orange solid (0.080 g, 55%). Mp 183 °C; FTIR (ATR, cm^{-1}) ν 2936, 2847, 1686, 1612, 1483, 1374, 1076, 831, 695. ^{1}H-NMR (600 MHz, $CDCl_3$, ppm) δ 7.76 (d, 4H, J = 8.4 Hz), 7.50 (d, 4H, J = 8.4 Hz), 3.72 (t, 4H, J = 7.5 Hz), 1.56 (m, 4H), 1.21 (m, 12H), 0.83 (t, 6H); ^{13}C-NMR (150 MHz, $CDCl_3$, ppm) δ 162.5, 147.4, 137.4, 130.0, 129.3, 136.6, 110.0, 41.9, 31.2, 29.7, 29.4, 26.4, 22.5, 13.9; *m*/*z* (HRMS MALDI-TOF) $C_{30}H_{34}Cl_2N_2O_2$ calcd 524.1997; found 524.4251 (M+).

3,6-Bis(4-chlorophenyl)-2,5-bis(6-(3,6-di-*tert*-butyl-carbazol-*N*-yl)hexyl)-2,5-dihydropyrrolo[3,4-*c*]pyrrole-1,4-dione (G1DPP). It was synthesized from compound **2** (0.372, 0.84 mmol), KO^{t}Bu

(0.0691 g, 0.62 mmol) and Pigment Red 254 (**5**) (0.10 g, 0.28 mmol) using the same conditions as that for **G0DPP** and obtained as an orange solid (0.15 g, 45%). Mp 192 °C; FTIR (ATR, cm^{-1}) ν 2950, 2868, 2311, 1673, 1605, 1475, 1353, 1082, 797, 716. ^{1}H-NMR (600 MHz, $CDCl_3$, ppm) δ 8.09 (s, 4H), 7.70 (d, 4H, $J = 8.4$ Hz), 7.45–7.49 (m, 8H), 7.23 (d, $J = 8.4$ Hz, 4H), 4.18 (t, 4H, $J = 6.8$ Hz), 3.69 (t, 4H, $J = 7.3$ Hz), 1.78 (m, 4H), 1.53 (m, 4H), 1.45 (m, 36H), 1.24–1.30 (m, 8H). ^{13}C-NMR (150 MHz, $CDCl_3$, ppm) δ 162.4, 147.3, 141.5, 138.9, 137.4, 129.9, 129.3, 126.4, 123.2, 122.7, 116.3, 109.9, 107.9, 42.9, 41.8, 34.7, 32.1, 29.3, 29.0, 26.8, 26.6; *m*/*z* (HRMS MALDI-TOF) $C_{70}H_{80}Cl_2N_4O_2$ calcd 1078.5658; found 1078.6823 (M+).

3,6-Bis(4-chlorophenyl)-2,5-bis(6-(3,3″,6,6″-tetra-*tert*-butyl-[*N*,3′:6′,*N*″-tercarbazol]-*N*′-yl)hexyl)-2,5-dihydropyrrolo[3,4-*c*]pyrrole-1,4-dione (G2DPP). It was synthesized from compound **4** (0.372, 0.42), KO^{t}Bu (0.035 g, 0.31 mmol) and Pigment Red 254 (**5**) (0.05 g, 0.14 mmol) using the same conditions as that for **G0DPP** and obtained as an orange solid (0.083 g, 52%). Mp 247 °C; FTIR (ATR, cm^{-1}) ν 2963, 2854, 2359, 1673, 1503, 1258, 811, 606. ^{1}H-NMR (600 MHz, $CDCl_3$, ppm) δ 8.17 (s, 4H), 8.15 (s, 8H), 7.73 (d, 4H, $J = 8.4$ Hz), 7.55–7.61 (m, 8H), 7.42–7.46 (d, 12H), 7.30 (d, 8H, $J = 8.4$ Hz), 4.40 (t, 4H, $J = 7.2$ Hz), 3.76 (m, 4H), 1.94–1.99 (m, 4H), 1.61–1.65 (m, 4H), 1.26–1.46 (m, 80H); ^{13}C-NMR (150 MHz, $CDCl_3$, ppm) δ 162.4, 147.3, 142.5, 140.3, 139.9, 137.5, 129.9, 129.4, 126.4, 125.7, 123.5, 123.1, 119.5, 116.2, 110.0, 109.8, 109.1, 43.4, 41.8, 34.7, 32.1, 29.4, 29.0, 26.8, 26.6; *m*/*z* (HRMS MALDI-TOF) $C_{134}H_{140}Cl_2N_8O_2$ calcd 1963.0476; found 1963.0941 (M+).

Results and discussion

Synthesis and characterization

The synthesis of di(*p*-chlorophenyl)-DPP (Pigment Red 254) functionalized with carbazole dendrons is outlined in Scheme 1. Firstly, the synthesized 3,6-di-*tert*-butylcarbazole (**1**) and 3,3″,6,6″-tetra-*tert*-butyl-*N*′,3′:6′,*N*″-tercarbazole (**3**)[50,52] were alkylated with an excess amount of 1,6-dibromohexane in the presence of KOH as a base in dimethylformamide to afford the monoalkylated molecules **2** and **4** in good yield, respectively. In the final step, alkylation of Pigment Red 254 (**5**) with 1-bromohexane, compound **2**, or compound **4** under basic conditions of KO^{t}Bu in *N*-methyl-2-pyrrolidone gave the desired products **G0DPP**, **G1DPP**, and **G2DPP** as yellow-orange solids in moderate yields, respectively. All molecules were chemically characterized by ^{1}H NMR, ^{13}C NMR, and high-resolution MALDI-TOF mass spectra, agreeing well with their proposed structures (Fig. S3–S7, ESI†). Due to the existence of a hexyl chain and carbazole dendron, the newly synthesized di(*p*-chlorophenyl)-DPP derivatives displayed good solubility in most organic solvents and could be processed into thin films using simple solution-processed casting methods.

Theoretical calculation

The electronic structure and molecular geometry were investigated using the density functional theory (DFT) method with the B3LYP hybrid function and 6-31G(d) basis set as implemented in Gaussian 09.[56] The optimized geometries of **G0DPP–G2DPP** revealed that the di(*p*-chlorophenyl)-DPP core adopts a planar conformation (Fig. S1, ESI†). In case of **G1DPP** and **G2DPP**, the core is sandwiched by pendant carbazole dendrons. The molecules become more hindered as the generation of dendrons increased due to the strongly twisted structure of each carbazole unit in the dendron. These structural characteristics can influence the physical properties of the material. The lowest unoccupied molecular orbital (LUMO) energy level of all the molecules was calculated to be approximately the same (−2.63 to −2.70 eV), while their highest occupied molecular orbital (HOMO) energy levels varied (−5.36 to −5.01 eV). A more detailed picture comparing the HOMO and LUMO for all three molecules is depicted in Fig. 1. As is evident from this picture, the LUMO orbitals of all the molecules are located on the electron-deficient di(*p*-chlorophenyl)-DPP core. The distribution of the π-electrons in the HOMO of **G0DPP** is on the DPP

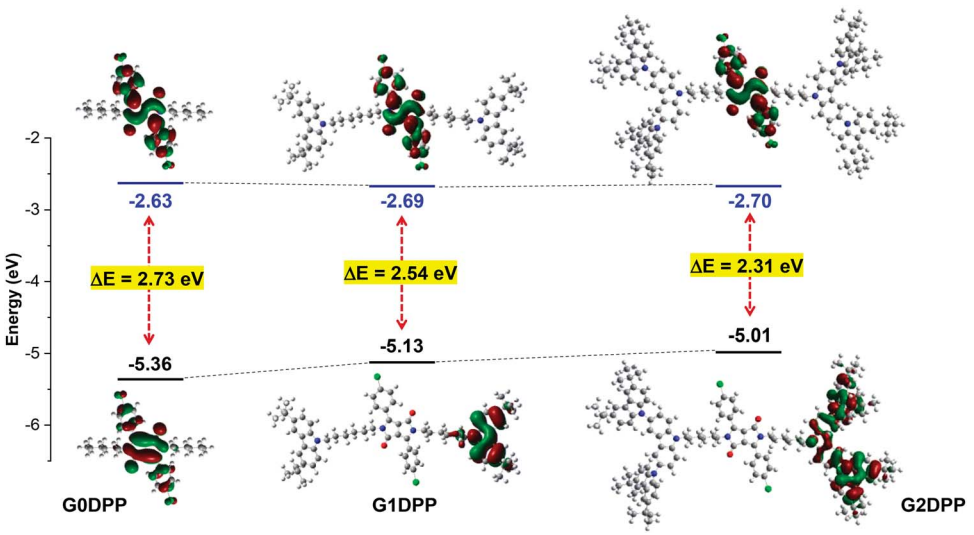

Fig. 1 Frontier-orbital distribution, HOMO and LUMO energy levels of G0DPP–G2DPP simulated using the B3LYP/6-31G(d) basis set.

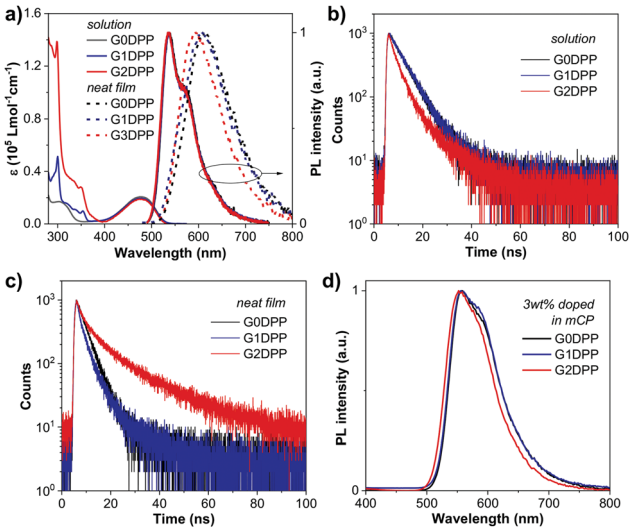

Fig. 2 (a) UV-vis absorption spectra in toluene solution and normalized PL spectra of **G0DPP–G2DPP** in toluene solution and thin film spin-coated on quartz substrates of **G0DPP–G2DPP**. Transient PL decay spectra of **G0DPP–G2DPP** (b) in toluene solution and (c) as neat films. (d) Normalized PL spectra of 3 wt% **G0DPP–G2DPP** doped in mCP.

orbitals, whereas the π-electrons are delocalized over the entire carbazole moieties in the case of **G1DPP** and **G2DPP**. Accordingly, the HOMO levels decreased with an increase in the generation of dendrons, while the LUMO levels remained unchanged. The low HOMO levels of both **G1DPP** (−5.13 eV) and **G2DPP** (5.01 eV) imply that they are susceptible to hole injection from the indium tin oxide (ITO) anode when fabricated as an emissive layer (EML) in OLED devices.

Optical properties

The UV-visible absorption spectra of the di(*p*-chlorophenyl)-DPP derivatives in toluene solution (10^{-6} M) are shown in Fig. 2a. The detailed optical data are summarized in Table 1. All the spectra showed the main broad absorption band maximum at 479 nm, which can be assigned to the π–π* transition of the di(*p*-chlorophenyl)-DPP moiety (Fig. 2a).[42] In **G1DPP** and **G2DPP**, a sharp absorption band at a lower wavelength (298 nm), corresponding to the π–π* transition of the carbazole moiety, was also observed. Noticeably, the DDP absorption peak intensities of all the molecules barely changed (Fig. 2a and Table 1), suggesting that grating the DPP core with electron-donating carbazole dendrons in a non-conjugated manner does not affect its electronic properties. This result is consistent with the constant in LUMO levels observed in the DFT calculation. Moreover, the intensity of the absorption peak at 298 nm increases from **G1DPP** to **G2DPP**, which is related to the increased number of carbazole units in the substituent moieties. Thus, the optical band gap (Eg^{opt}) of these molecules will not be affected. As depicted in Table 1, the Eg^{opt} values calculated from the onset of the absorption spectra are 2.33 eV for **G0DPP**, 2.34 eV for **G1DPP**, and 2.35 eV for **G2DPP**. In solution, **G0DPP–G2DPP** demonstrated a strong yellow emission with an absolute PL quantum yield (Φ_{PL}) close to unity (Table 1). They showed identical photoluminescence (PL) spectra with peaks at 536 and 578sh nm, which are attributed to the emission of the di(*p*-chlorophenyl)-DPP core (Fig. 2a). The PL spectra of **G1DPP** and **G2DPP** are excitation wavelength independent, where excitation occurs either at the carbazole moieties (at 298 nm) or DDP core (at 479 nm), and thus the PL spectra obtained are identical. The results suggest that energy or excitons can efficiently be transferred from the carbazole moiety to the emissive DPP unit. In the neat film, the PL spectra displayed a large bathochromic-shift compared to the PL in solution, indicating the substantial aggregation of the molecule in the film state. **G0DPP**, in particular, its PL spectrum was red-shifted to 610 nm and became broad with a featureless band. **G2DPP** bearing a 2nd carbazole dendron exhibited weaker intermolecular aggregation. Consequently, the Φ_{PL} values of these compounds doped in the neat film were as low as 9–20% (Table 1). The transient PL decay spectra of **G0DPP–G2DPP** in solution and neat film are shown in Fig. 2b and c, and the lifetimes are listed in Table 1, respectively. In both conditions, all the molecules displayed only prompt fluorescence with a short lifetime (ns). It is interesting to note that the PL lifetime of **G2DPP** in the neat film (13

Table 1 Key physical data of the synthesized compounds

Compd	λ_{abs} (log ε)[a] (nm, M^{-1} cm^{-1})	λ_{em} (nm) sol[a]/film[b]/dfilm[c]	τ[d] (ns) sol[b]/film[b]	T_{5d}[e] (°C)	$E_{1/2}$ *vs.* Ag/Ag^{+}[f] (V)	Φ_{PL}[g] (%) sol[a]/film[b]/dfilm[c]	Eg^{opt}[h] (eV)	HOMO/LUMO/E_g^{ele}[i] (eV)	LUMO[j] (eV)	Hole mobility[k] (cm^2 V^{-1} s^{-1})
G0DPP	479 (4.31)	536/610/557	6/4	356	−1.73, −1.2, 1.23, 1.47	96/9/67	2.33	−5.69/−3.33/2.36	3.34	2.00×10^{-6}
G1DPP	298 (4.71), 479 (4.29)	536/608/557	6/4	409	−1.75, −1.19, 1.15, 1.52	95/12/71	2.34	−5.51/−3.33/2.18	3.16	2.56×10^{-6}
G2DPP	298 (5.14), 479 (4.27)	536/595/553	6/13	432	−1.76, −1.18, 1.02, 1.20, 1.50	92/20/70	2.35	−5.29/−3.33/1.96	2.94	3.35×10^{-5}

[a] Measured in toluene. [b] Measured as the neat film. [c] Measured as 3 wt% doped in mCP thin film. [d] Transient PL decay time. [e] Analysed by TGA at a heating rate of 10 °C min^{-1} under an N_2 flow. [f] Obtained from CV at a scan rate of 50 mV s^{-1} in CH_2Cl_2 and n-Bu_4NPF_6 as the electrolyte. [g] Absolute PL quantum yield measured by integrating sphere. [h] Estimated from the optical absorption edge, $Eg^{opt} = 1240/\lambda_{onset}$. [i] Calculated using HOMO = −(4.44 + Eo^{ox}_{nset}); LUMO = −(4.44 + Eo^{re}_{nset}); $E_g^{ele} = Eo^{ox}_{nset} - Eo^{re}_{nset}$, where Eo^{ox}_{nset} is the onset potential of the oxidation and Eo^{re}_{nset} is the onset potential of the reduction. [j] LUMO = HOMO − Eg^{opt}. [k] Obtained from hole-only device (ITO/PEDOT:PSS/Compd/MoO_3/Al).

ns) was somewhat longer than in solution. This can be attributed to the fact that the bulky molecular structure of the 2nd carbazole dendron hampers the π-stacked aggregation of the di(*p*-chlorophenyl)-DPP core in the solid state, leading to less planarization of the molecule, and thus giving rise to a long PL lifetime.[57] Thus, to improve the Φ_{PL}s of **G0DPP–G2DPP** in the film state, they were doped in the mCP host matrix. With the optimum doping concentration of 3 wt% of the compound in CBP, the thin films exhibited strong yellow emissions, with the Φ_{PL} values insignificantly enhanced up to 71% (Table 1). As shown in Fig. 2d, the PL spectra of all the doped thin films display pure dopant emissions peaked at 553–557 nm, which are slightly blue-shifted compared to that in the PL spectrum of the corresponding neat film. These results imply that doping of the compounds in the mCP host matrix well suppresses molecular aggregation and restores their high Φ_{PL} as that in solution.

Thermal and electrochemical properties and hole mobility

The thermal properties of **G0DPP–G2DPP** were investigated by thermal gravimetric analysis (TGA), which revealed that all the molecules exhibit high thermal stability with decomposition temperatures at 5% weight loss (T_{5d}) of over 356 °C (Fig. 3a and Table 1).

The electrochemical properties of the samples were explored by cyclic voltammetry (CV) to estimate the oxidation, reduction potentials, and HOMO–LUMO energy levels of each molecule. The experiments were performed in CH_2Cl_2 solution with 0.1 M *n*-Bu_4NPF_6 as the supporting electrolyte. The CV plots of **G0DPP–G2DPP** are shown in Fig. 3a, and the data is tabulated in Table 1. All the compounds displayed multiple oxidation and reduction processes. Their reductions occurred at the same reduction half-wave potentials ($E_{1/2}$) of ∼−1.2 and ∼−1.7 V, which are attributed to the reduction of the di(*p*-chlorophenyl)-DPP moiety.[42] The oxidations at $E_{1/2}$ of ∼1.2 and ∼1.5 V can also be ascribed to the oxidation of the DPP core. Thus, the oxidation wave at the lower potential of 1.15 V for **G1DPP** and 1.02 for **G2DPP** can be related to the oxidation of the grafting carbazole dendrons. Moreover, the CV traces remained unchanged in their continual CV scans, proving the high electrochemical stability of these molecules. Subsequently, the HOMOs, LUMOs, and band gaps were deduced from the oxidation onset (Eo^{ox}_{nset}) and reduction onset (Eo^{re}_{nset}) following the equations described in the footnote of Table 1. Although optical band gaps for all three materials were found to be identical, the electrochemical HOMO and LUMO values and electrochemical band gaps (E^{ele}_g) varied among the molecules. These values are compared in Table 1. **G2DPP** was found to have the smallest E^{ele}_g value (1.96 eV) and also the lowest-lying LUMO level (−5.29 eV). Upon going from the unsubstituted hexyl chain (**G0DPP**) to the 1st generation carbazole dendron (**G1DPP**) and 2nd generation carbazole dendron (**G2DPP**), the trend of increasing HOMO energy was observed, and thus narrowing of the bandgap. These electrochemical results are similar to the calculated HOMO, LUMO, and Δ*E* values calculated in the DFT experiment. The presence of the carbazole dendron is innately likely to make the molecules easier to oxidize. The LUMO levels of the compounds were calculated using the difference between the optical band gap (Eg^{opt}) and HOMO level obtained from electrochemical measurements and are listed in Table 1. Markedly, the HOMO levels of **G1DPP** and **G2DPP** are close to the work function of the ITO/PEDOT:PSS anode (5.20 eV) (Fig. 5a),[58] and as an emissive layer, they can be coated on top of the ITO/PEDOT:PSS anode without any assistance from hole-injection materials (HIM) and hole-transporting materials (HTM), giving rise to a simple device architecture.

The hole-transporting ability of **G0DPP–G2DPP** was also determined using the space charge limited current (SCLC) method based on the current density–voltage (*J–V*) measurements of a hole-only device (ITO/PEDOT:PSS (35 nm)/**G0DPP–G2DPP** (100 nm)/MoO_3 (10 nm)/Al (100 nm))[59] (Fig. 4). The hole mobilities of **G0DPP–G2DPP** were estimated by combining the Mott–Gurney equation and Frenkel effect[60] to be in the range of 2.00×10^{-6} to 3.35×10^{-5} $cm^2\ V^{-1}\ s^{-1}$ (Table 1). Among them, **G2DPP** possessed the highest hole mobility of 3.35×10^{-5} $cm^2\ V^{-1}\ s^{-1}$. This high hole mobility can be beneficial for high-performance OLED devices.[61] It has been established that

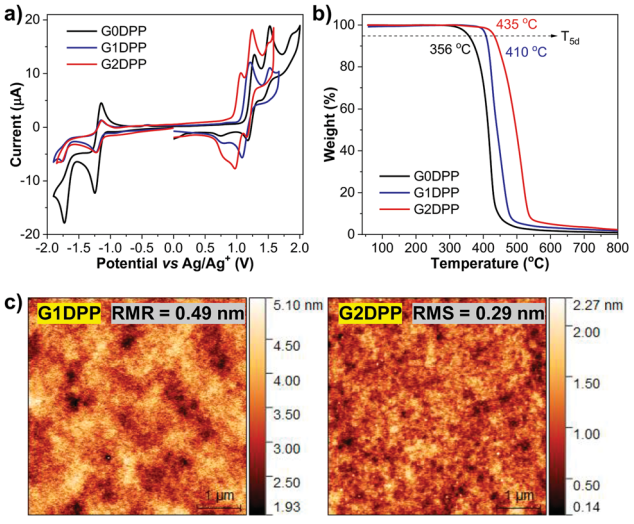

Fig. 3 (a) TGA plots of **G0DPP–G2DPP** analyzed under N_2 at a heating rate of 10 °C min^{-1}. (b) CV curves of **G0DPP–G2DPP** measured in CH_2Cl_2 solution containing 0.1 M Bu_4NPF_6 at a scan rate of 50 mV s^{-1}. (c) AFM images of **G1DPP** and **G2DPP** 3 wt% doped in mCP thin films.

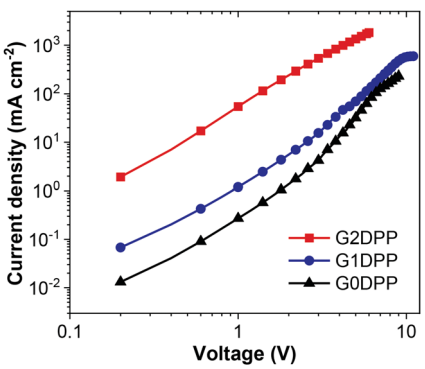

Fig. 4 Current density–voltage (*J–V*) plots of the hole-only devices.

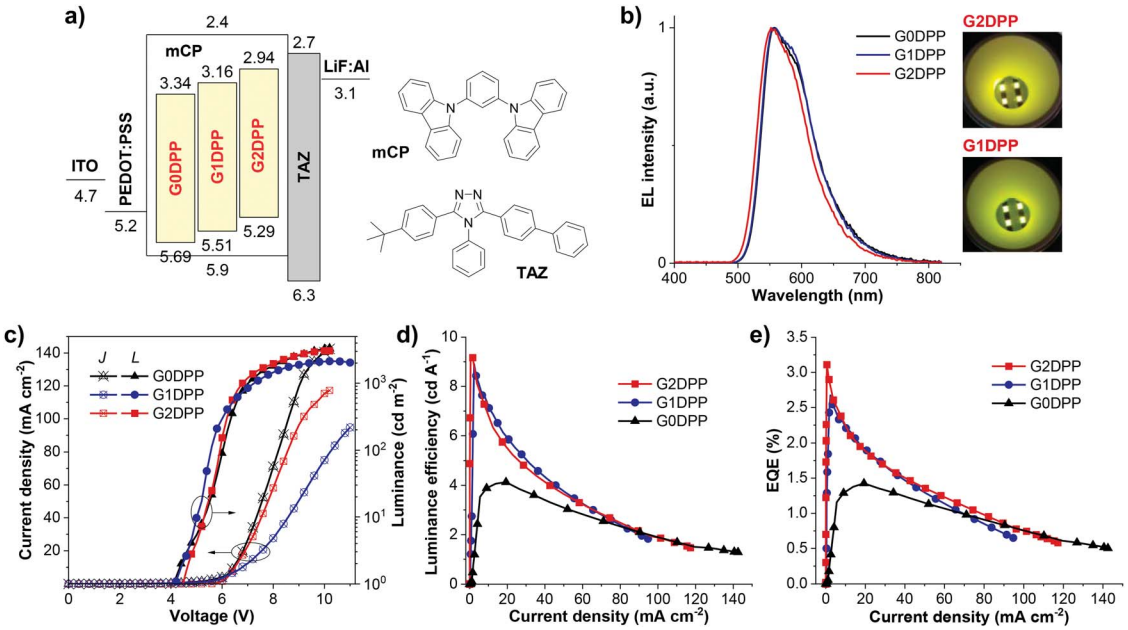

Fig. 5 (a) Device structure and energy levels (relative to the vacuum energy level) of the materials used. (b) Normalized EL spectra (inset: photographs of yellow **G1DPP** and **G2DPP**-based OLEDs), (c) current density–voltage–luminance (*J*–*V*–*L*) plots, (d) luminance efficiency–current density (CE–*J*) plots and (e) external quantum efficiency–current density (EQE–*J*) plots of the fabricated **G0DPP–G3DPP**-based OLEDs.

high mobility emitters can widen the recombination zone in the emissive layer and result in a longer device lifetime and lower driving voltages.[61,62]

Electroluminescent properties

To evaluate the electroluminescence properties of the newly synthesized di(*p*-chlorophenyl)-DPP derivatives, OLED devices with the optimized structure of indium tin oxide (ITO)/PEDOT:PSS (35 nm)/EML (35 nm)/TAZ (40 nm)/LiF (0.5 nm) : Al (150 nm) were fabricated. The EML was spin-coated from a $CHCl_3$–toluene (1 : 1) solution of **G0DPP–G2DPP** 3 wt% in mCP with a controllable thickness. The morphology of the casted thin films was studied by atomic force microscopy (AFM), which showed that they all displayed amorphous features with uniform smooth surfaces and root-mean-square roughness (RMS) values of less than 1 nm (Fig. 3c). The surface was observed to have no pinholes and crystalline islands, indicating high-quality nanoscale thin films. To realize the optimal device performance from the EML, TAZ was utilized as an electron-transporting layer (ETL) and hole blocking layer (HBL). As shown in Fig. 5a, the suitable LUMO level of TAZ and its high electron mobility can enable the control and enhancement of the electron–hole recombination zone in the EML,[63] whereas the large energy barrier between the HOMOs of the EML and the ETL will confine hole accumulation and exciton recombination close to this interface.[64,65] The electroluminescence (EL) spectra, current density–voltage-luminance (*J*–*V*–*L*) plots, current density dependence of the luminance efficiency (LE) and external quantum efficiency (EQE) of the devices are shown in Fig. 5b–e, and the essential EL data is summarized in Table 2.

Under an applied voltage, all the devices (I, II, and III) emitted intense yellow EL emission colors peaked at 553–556 nm, as shown in Fig. 5b and the inset. The EL spectra overlapped well with the PL spectra of the EML in a thin film with no emission peaks from the mCP host matrix (404 and 426 nm)[66,67] and TAZ layer (380 nm),[67] indicating that the EL is purely the emissions from the EML. Remarkably, for each device, the shape and maximum wavelength of its EL spectrum remained unchanged with an increase in applied voltage from 7 V to 11 V (Fig. S2, ESI†). This implies efficient charge injection and recombination in the EML, and the excimer emission and exciplex emissions from the EML/TAZ interface are effectively repressed. All the devices were confirmed to be well-balanced and optimized for both charge transport and energy transfer

Table 2 Electroluminescent data of the fabricated OLED devices[a]

Device	EML	V_{on}[b] (V)	λ_{max}^{EL} (nm)	FWHM (nm)	L_{max}[c] (cd m^{-2})	J_{max}[d] (mA cm^{-2})	CE_{max}[e] (cd A^{-1})	EQE_{max}[f] (%)	CIE (*x*,*y*)
I	**G0DPP**	4.2	556	88	3376	142	4.13	1.42	0.48, 0.51
II	**G1DPP**	4.2	556	88	2034	95	8.91	2.67	0.48, 0.51
III	**G2DPP**	4.5	553	84	3060	117	9.24	3.11	0.45, 0.53

[a] ITO/PEDOT:PSS/EML 3 wt% in mCP/TAZ/LiF : Al. [b] Turn-on voltage at 1 cd m^{-2}. [c] Maximum luminance. [d] Current density at maximum luminance. [e] Maximum luminous efficiency. [f] Maximum external quantum efficiency.

from the mCP host to the **G0DPP–G2DPP** dopants and operated stably. Among the three devices, device III having **G2DPP** as the EML exhibited the best EL performance with a maximum luminance of 3060 cd m^{-2}, maximum LE of 9.24 cd A^{-1}, maximum EQE of 3.11%, and turn-on voltage (V_{on}) of 4.5 V. Device II using **G1DPP** as the EML showed a slightly lower device EL performance with a maximum luminance of 2034 cd m^{-2} and maximum LE and EQE values of 8.91 cd A^{-1} and 2.67%, respectively. The **G0DPP**-based OLED (device I) exhibited the lowest EL performance with the maximum LE and EQE values of 4.13 cd A^{-1} and 1.42%, respectively. According to these results, the performance of the devices (V_{on}, LE, and EQE values) decreased in the order of III > II > I, following a similar trend for the hole mobility of the EML materials, which was observed to be **G2DPP** > **G1DPP** > **G0DPP**. It is well-known that a high mobility EML material can widen the recombination zone in the emissive layer and result in a longer device lifetime and lower driving voltages.[68] Thus, the outstanding EL performance of the **G2DPP** emitter can be ascribed to the combination of its high thin film Φ_{PL}, high hole mobility, and suitable HOMO/LUMO levels, ensuring more balanced and improved recharge recombination behavior within the device.[69]

Conclusions

In conclusion, we reported the design strategy and synthesis of new di(*p*-chlorophenyl)-DPP derivatives (**G0DPP–G2DPP**) for use as emissive materials in OLEDs. The molecules were grafted with a series of hole-transporting carbazole dendrons on the DPP core through a hexyl chain linkage to enhance their hole-transporting property and electroluminescent performance in the devices. Owing to the non-conjugated link between the carbazole dendrons and DPP core, they exhibited a slight effect on the optical and electronic properties of the molecules, as expected. Moreover, the carbazole dendron not only assembled in a bulky geometry in the molecules but also enhanced their hole-transporting ability. Because of their weak molecular interactions, these materials exhibited decent thermal stability, good thin film-forming capability, and high photoluminescence quantum yield in the film state. Especially, **G2DPP** carrying the 2^{nd} generation carbazole dendron as the grating moiety exhibited high hole mobility and realized an excellent electroluminescent performance in a solution-processed double-layered OLED. The device displayed a strong and stable yellow emission color with a brightness of 3060 cd m^{-2}, maximum LE of 9.24 cd A^{-1}, and maximum EQE of 3.11%. It is believed that this work can present a useful methodology to decorate DPP as an efficient light-emitting material with a hole-transporting facet for acquiring simple-structured OLEDs. This work also ascertained that carbazole dendrons can be a worthwhile moiety capable of being exploited for the development of solution-processed hole-transporting emissive compounds.

Author contributions

W. K. performed the synthesis and characterizations of the materials, discussed the data, and prepared the original draft. S. N. and P. C. performed the quantum chemical calculations and analyzed the data. T. C. and T. S. completed the device fabrication and analyzed the data. V. P. and T. M. conceived and supervised the project and review & editing the final draft. All authors approved the final version of the manuscript.

Conflicts of interest

There are no conflicts to declare.

Acknowledgements

This work was financially supported by the National Research Council of Thailand and Suranaree University of Technology (Grant No. 10/9/1-2561). Many thanks also go to the Thailand Research Fund (RTA6080005) and the National Nanotechnology Center, NSTDA, Ministry of Higher Education, Science, Research and Innovation, Thailand, through its program of Research Network National Nanotechnology Center for the supports. We also gratefully acknowledge the graduate fellowship support for W. K. from Udon Thani Rajabhat University (UDRU).

Notes and references

1 C. W. Tang and S. A. Vanslyke, *Appl. Phys. Lett.*, 1987, **51**, 913–915.
2 H. Jia, *Natl. Sci. Rev.*, 2018, **5**, 427–431.
3 P. Therdkatanyuphong, P. Chasing, C. Kaiyasuan, S. Boonnab, T. Sudyoadsuk and V. Promarak, *Adv. Funct. Mater.*, 2020, **30**, 2002481.
4 F. So, J. Kido and P. Burrows, *MRS Bull.*, 2008, **33**, 663–669.
5 U. Mitschke and P. Bäuerle, *J. Mater. Chem.*, 2000, **10**, 1471–1507.
6 A. Kumar, W. Lee, T. Lee, J. Jung, S. Yoo and M. H. Lee, *J. Mater. Chem. C*, 2020, **8**, 4253–4263.
7 D. H. Ahn, S. W. Kim, H. Lee, I. J. Ko, D. Karthik, J. Y. Lee and J. H. Kwon, *Nat. Photonics*, 2019, **13**, 540–546.
8 L. Yu, Z. Wu, G. Xie, W. Zeng, D. Ma and C. Yang, *Chem. Sci.*, 2018, **9**, 1385–1391.
9 X. Liu, B. Yao, Z. Zhang, X. Zhao, B. Zhang, W. Y. Wong, Y. Cheng and Z. Xie, *J. Mater. Chem. C*, 2016, **4**, 5787–5794.
10 P. Funchien, P. Chasing, T. Sudyoadsuk and V. Promarak, *Chem. Commun.*, 2020, **56**, 6305–6308.
11 S. M. Russell, A. M. Brewer, D. M. Stoltzfus, J. Saghaei and P. L. Burn, *J. Mater. Chem. C*, 2019, **7**, 4681–4691.
12 M. Kim, S. K. Jeon, S. H. Hwang and J. Y. Lee, *Adv. Mater.*, 2015, **27**, 2515–2520.
13 Z. Hao and A. Iqbal, *Chem. Soc. Rev.*, 1997, **26**, 203.
14 Q. Liu, S. E. Bottle and P. Sonar, *Adv. Mater.*, 2020, **32**, 1903882.
15 M. Kaur and D. H. Choi, *Chem. Soc. Rev.*, 2015, **44**, 58–77.
16 C. B. Nielsen, M. Turbiez and I. McCulloch, *Adv. Mater.*, 2013, **25**, 1859–1880.
17 Y. Li, P. Sonar, L. Murphy and W. Hong, *Energy Environ. Sci.*, 2013, **6**, 1684–1710.

18 L. Biniek, B. C. Schroeder, C. B. Nielsen and I. McCulloch, *J. Mater. Chem.*, 2012, **22**, 14803–14813.
19 B. Walker, J. Liu, C. Kim, G. C. Welch, J. K. Park, J. Lin, P. Zalar, C. M. Proctor, J. H. Seo, G. C. Bazan and T. Q. Nguyen, *Energy Environ. Sci.*, 2013, **6**, 952–962.
20 Z. Yi, S. Wang and Y. Liu, *Adv. Mater.*, 2015, **27**, 3589–3606.
21 Y. Qu, Y. Wu, Y. Gao, S. Qu, L. Yang and J. Hua, *Sens. Actuators, B*, 2014, **197**, 13–19.
22 G. Zhang, S. Bi, L. Song, F. Wang, J. Yu and L. Wang, *Dyes Pigm.*, 2013, **99**, 779–786.
23 M. Kaur, M. J. Cho and D. H. Choi, *Dyes Pigm.*, 2014, **103**, 154–160.
24 Y. H. Jeong, C. H. Lee and W. D. Jang, *Chem.–Asian J.*, 2012, **7**, 1562–1566.
25 W. Li, L. Wang, H. Tang and D. Cao, *Dyes Pigm.*, 2019, **162**, 934–950.
26 C. Du, S. Fu, X. Wang, A. C. Sedgwick, W. Zhen, M. Li, X. Li, J. Zhou, Z. Wang, H. Wang and J. L. Sessler, *Chem. Sci.*, 2019, **10**, 5699–5704.
27 E. Q. Guo, P. H. Ren, Y. L. Zhang, H. C. Zhang and W. J. Yang, *Chem. Commun.*, 2009, 5859–5861.
28 A. Nowak-Król, M. Grzybowski, J. Romiszewski, M. Drobizhev, G. Wicks, M. Chotkowski, A. Rebane, E. Górecka and D. T. Gryko, *Chem. Commun.*, 2013, **49**, 8368–8370.
29 S. Qu and H. Tian, *Chem. Commun.*, 2012, **48**, 3039–3051.
30 J. Liu, Y. Zhang, H. Phan, A. Sharenko, P. Moonsin, B. Walker, V. Promarak and T.-Q. Nguyen, *Adv. Mater.*, 2013, **25**, 3645–3650.
31 Y. Farré, L. Zhang, Y. Pellegrin, A. Planchat, E. Blart, M. Boujtita, L. Hammarström, D. Jacquemin and F. Odobel, *J. Phys. Chem. C*, 2016, **120**, 7923–7940.
32 K. Aoshima, M. Ide and A. Saeki, *RSC Adv.*, 2018, **8**, 30201–30206.
33 J. C. Bijleveld, A. P. Zoombelt, S. G. J. Mathijssen, M. M. Wienk, M. Turbiez, D. M. de Leeuw and R. A. J. Janssen, *J. Am. Chem. Soc.*, 2009, **131**, 16616–16617.
34 C. Zhao, Y. Guo, Y. Zhang, N. Yan, S. You and W. Li, *J. Mater. Chem. A*, 2019, **7**, 10174–10199.
35 K. Gao, S. B. Jo, X. Shi, L. Nian, M. Zhang, Y. Kan, F. Lin, B. Kan, B. Xu, Q. Rong, L. Shui, F. Liu, X. Peng, G. Zhou, Y. Cao and A. K. Y. Jen, *Adv. Mater.*, 2019, **31**, 1807842.
36 L. Huo, J. Hou, H. Y. Chen, S. Zhang, Y. Jiang, T. L. Chen and Y. Yang, *Macromolecules*, 2009, **42**, 6564–6571.
37 B. Tieke, A. R. Rabindranath, K. Zhang and Y. Zhu, *Beilstein J. Org. Chem.*, 2010, **6**, 830–845.
38 O. Fenwick, S. Fusco, T. N. Baig, F. Di Stasio, T. T. Steckler, P. Henriksson, C. Fléchon, M. R. Andersson and F. Cacialli, *APL Mater.*, 2013, **1**, 032108.
39 M. Sassi, N. Buccheri, M. Rooney, C. Botta, F. Bruni, U. Giovanella, S. Brovelli and L. Beverina, *Sci. Rep.*, 2016, **6**, 34096.
40 Y. Zhu, A. R. Rabindranath, T. Beyerlein and B. Tieke, *Macromolecules*, 2007, **40**, 6981–6989.
41 G. Wiosna-Salyga, M. Gora, M. Zagorska, P. Toman, B. Luszczynska, J. Pfleger, I. Glowacki, J. Ulanski, J. Mieczkowski and A. Pron, *RSC Adv.*, 2015, **5**, 59616–59629.
42 E. D. Głowacki, H. Coskun, M. A. Blood-Forsythe, U. Monkowius, L. Leonat, M. Grzybowski, D. Gryko, M. S. White, A. Aspuru-Guzik and N. S. Sariciftci, *Org. Electron.*, 2014, **15**, 3521–3528.
43 A. Van Dijken, J. J. A. M. Bastiaansen, N. M. M. Kiggen, B. M. W. Langeveld, C. Rothe, A. Monkman, I. Bach, P. Stössel and K. Brunner, *J. Am. Chem. Soc.*, 2004, **126**, 7718–7727.
44 H. Huang, X. Yang, B. Pan, L. Wang, J. Chen, D. Ma and C. Yang, *J. Mater. Chem.*, 2012, **22**, 13223–13230.
45 S. W. Li, C. H. Yu, C. L. Ko, T. Chatterjee, W. Y. Hung and K. T. Wong, *ACS Appl. Mater. Interfaces*, 2018, **10**, 12930–12936.
46 M. Godumala, S. Choi, M. J. Cho and D. H. Choi, *J. Mater. Chem. C*, 2019, **7**, 2172–2198.
47 D. Xia, B. Wang, B. Chen, S. Wang, B. Zhang, J. Ding, L. Wang, X. Jing and F. Wang, *Angew. Chem., Int. Ed.*, 2014, **53**, 1048–1052.
48 T. Keawin, N. Prachumrak, S. Namuangruk, S. Pansay, N. Kungwan, S. Maensiri, S. Jungsuttiwong, T. Sudyoadsuk and V. Promarak, *RSC Adv.*, 2015, **5**, 73481–73489.
49 J. You, G. Li and Z. Wang, *Polymer*, 2012, **53**, 5116–5123.
50 P. Moonsin, N. Prachumrak, R. Rattanawan, T. Keawin, S. Jungsuttiwong, T. Sudyoadsuk and V. Promarak, *Chem. Commun.*, 2012, **48**, 3382–3384.
51 N. Prachumrak, S. Pansay, S. Namuangruk, T. Kaewin, S. Jungsuttiwong, T. Sudyoadsuk and V. Promarak, *Eur. J. Org. Chem.*, 2013, 6619–6628.
52 P. Moonsin, N. Prachumrak, S. Namuangruk, S. Jungsuttiwong, T. Keawin, T. Sudyoadsuk and V. Promarak, *Chem. Commun.*, 2013, **49**, 6388–6390.
53 T. Sudyoadsuk, P. Moonsin, N. Prachumrak, S. Namuangruk, S. Jungsuttiwong, T. Keawin and V. Promarak, *Polym. Chem.*, 2014, **5**, 3982–3993.
54 N. Prachumrak, S. Pojanasopa, S. Namuangruk, T. Kaewin, S. Jungsuttiwong, T. Sudyoadsuk and V. Promarak, *ACS Appl. Mater. Interfaces*, 2013, **5**, 8694–8703.
55 X. Li, J. Wang, R. Mason, X. R. Bu and J. Harrison, *Tetrahedron*, 2002, **58**, 3747–3753.
56 M. J. Frisch, G. W. Trucks, H. B. Schlegel, G. E. Scuseria, M. A. Robb, J. R. Cheeseman, G. Scalmani, V. Barone, G. A. Petersson, H. Nakatsuji, X. Li, M. Caricato, A. Marenich, J. Bloino, B. G. Janesko, R. Gomperts, B. Mennucci, H. P. Hratchian, J. V. Ortiz, A. F. Izmaylov, J. L. Sonnenberg, D. Williams-Young, F. Ding, F. Lipparini, F. Egidi, J. Goings, B. Peng, A. Petrone, T. Henderson, D. Ranasinghe, V. G. Zakrzewski, J. Gao, N. Rega, G. Zheng, W. Liang, M. Hada, M. Ehara, K. Toyota, R. Fukuda, J. Hasegawa, M. Ishida, T. Nakajima, Y. Honda, O. Kitao, H. Nakai, T. Vreven, K. Throssell, J. A. Montgomery, Jr., J. E. Peralta, F. Ogliaro, M. Bearpark, J. J. Heyd, E. Brothers, K. N. Kudin, V. N. Staroverov, T. Keith, R. Kobayashi, J. Normand, K. Raghavachari, A. Rendell, J. C. Burant, S. S. Iyengar, J. Tomasi, M. Cossi, J. M. Millam, M. Klene, C. Adamo, R. Cammi, J. W. Ochterski, R. L. Martin, K. Morokuma, O. Farkas,

J. B. Foresman and D. J. Fox, *Gaussian 09, Revision A.02*, Gaussian, Inc., Wallin, 2016.
57 K. Ji, Y. Xue and Z. Cui, *Opt. Mater.*, 2015, **47**, 180–184.
58 J. Wei, D. Bai and L. Yang, *PLoS One*, 2015, **10**, e0133725.
59 H. Li, L. Duan, D. Zhang and Y. Qiu, *J. Phys. Chem. C*, 2014, **118**, 9990–9995.
60 C. Katagiri, T. Yoshida, M. S. White, C. Yumusak, N. S. Sariciftci and K. I. Nakayama, *AIP Adv.*, 2018, **8**, 105001.
61 S. W. Culligan, A. C.-A. Chen, J. U. Wallace, K. P. Klubek, C. W. Tang and S. H. Chen, *Adv. Funct. Mater.*, 2006, **16**, 1481–1487.
62 J. H. Jou, S. Kumar, M. Singh, Y. H. Chen, C. C. Chen and M. T. Lee, *Molecules*, 2015, **20**, 13005–13030.
63 P. J. Jesuraj, H. Hafeez, D. H. Kim, J. C. Lee, W. H. Lee, D. K. Choi, C. H. Kim, M. Song, C. S. Kim and S. Y. Ryu, *J. Phys. Chem. C*, 2018, **122**, 2951–2958.
64 Z. B. Wang, M. G. Helander, Z. W. Liu, M. T. Greiner, J. Qiu and Z. H. Lu, *Appl. Phys. Lett.*, 2010, **96**, 043303.
65 Q. Wang, Q. S. Tian, Y. L. Zhang, X. Tang and L. S. Liao, *J. Mater. Chem. C*, 2019, **7**, 11329–11360.
66 J. G. Jang and H. J. Ji, *Adv. Mater. Sci. Eng.*, 2012, 192731.
67 T. Y. Cheng, J. H. Lee, C. H. Chen, P. H. Chen, P. S. Wang, C. E. Lin, B. Y. Lin, Y. H. Lan, Y. H. Hsieh, J. J. Huang, H. F. Lu, I. Chao, M. kit Leung, T. L. Chiu and C. F. Lin, *Sci. Rep.*, 2019, **9**, 3654.
68 S. W. Culligan, A. C. A. Chen, J. U. Wallace, K. P. Klubek, C. W. Tang and S. H. Chen, *Adv. Funct. Mater.*, 2006, **16**, 1481–1487.
69 S. Wehrmeister, L. Jäger, T. Wehlus, A. F. Rausch, T. C. G. Reusch, T. D. Schmidt and W. Brütting, *Phys. Rev. Appl.*, 2015, **3**, 024008.